Special Issue on CAD/Graphics 2017

Multi-scale geometry detail recovery on surfaces via Empirical Mode Decomposition

CrossMark

Xiaochao Wang [a,c], Jianping Hu [b,c,*], Dongbo Zhang [c], Lixin Guo [c], Hong Qin [d], Aimin Hao [c]

[a] School of Science, Tianjin Polytechnic University, Tianjin 300387, China
[b] College of Sciences, Northeast Electric Power University, Jilin 132012, China
[c] State Key Laboratory of Virtual Reality Technology and Systems, Beihang University, Beijing 100191, China
[d] Department of Computer Science, Stony Brook University, Stony Brook, NY 11794-4400, USA

ABSTRACT

In this paper, to recover the missing geometry details on 3D surfaces, we develop a novel geometry detail recovery algorithm for 3D surfaces based on Empirical Mode Decomposition (EMD). EMD is a powerful tool for processing non-linear and non-stationary signals and has been successfully used in 3D surface analysis and processing. Given a signal defined on 3D surface, EMD could represent the signal in a multi-scale fashion and decompose the signal into a number of Intrinsic Mode Functions (IMFs) and a residue, which usually encode the multi-level finer-scale details and the overall shape of the signal, respectively. Benefiting from the multi-scale representation of geometry details, the EMD-based multi-scale geometry detail recovery algorithm is developed. Our strategy starts from an initial smooth filling of a hole and then transfers the desirable details from the most similar region to the smoothly-filled surface within the framework of EMD. Taking the advantages of EMD, we first apply EMD on the whole completed surface to obtain the multi-scale representation of geometry details. Then, the most similar region corresponding to the hole region is located by the patch descriptor constructed from Heat Kernel Signature (HKS). Finally, the missing geometry details can be effectively recovered by transferring the geometry details from the found similar region to the smoothly-filled surface. Traditional methods, such as context-based methods or example-based methods, usually cut the similar patch and paste them onto the hole region, and they require to match with the hole boundary, are complex in general. In contrast, our method is simple and can transfer different scale details individually or in a concerted way, which makes our algorithm more flexible and can achieve versatile detail recovery results. Comprehensive experiments and quantitative comparisons on popular models have been used to demonstrate the effectiveness of our EMD-based multi-scale geometry detail recovery algorithm.

© 2017 Elsevier Ltd. All rights reserved.

1. Introduction and motivation

With the rapid development of 3D digitization technologies, 3D shapes can be easily acquired and applied in many applications, such as biomedicine, cultural heritage, 3D printing, architecture and construction, entertainment, etc. Due to complexity of shapes, and lack of scan views, the acquired point clouds usually contain missing regions, which result in many holes after reconstruction. Incomplete shapes limit the capabilities of downstream geometry algorithms and may influence the analysis and processing results.

Additionally, surface editing operations can also lead to holes on surfaces, where some parts of surface are removed. Therefore, it is highly desirable to fill the holes in a manner that produces complete geometry shapes.

For recovering the missing shape of 3D surfaces, there are a large number of hole-filling algorithms having been proposed, which can be generally classified into two categories: volume-based methods and mesh-based methods. Volume-based methods [1–7] have to resort to an intermediate volumetric grid, which can deal with complex holes, but it cannot preserve the sharp feature and geometric details well. Comparing with volume-based methods, mesh-based methods complete the hole directly on local mesh, and have been paid more attentions [8–25]. Most of these methods can successfully repair smooth surfaces, however, in real world there are plenty of models that are highly-detailed with rich features. Therefore, it is strongly desirable to recover the geome-

* Corresponding author at: College of Sciences, Northeast Electric Power University, Jilin 132012, China.
E-mail addresses: wangxiaochao18@gmail.com (X. Wang), neduhjp307@163.com (J. Hu), zhangdongbo9212@163.com (D. Zhang), guolx@buaa.edu.cn (L. Guo), qin@cs.stonybrook.edu (H. Qin), ham@buaa.edu.cn (A. Hao).
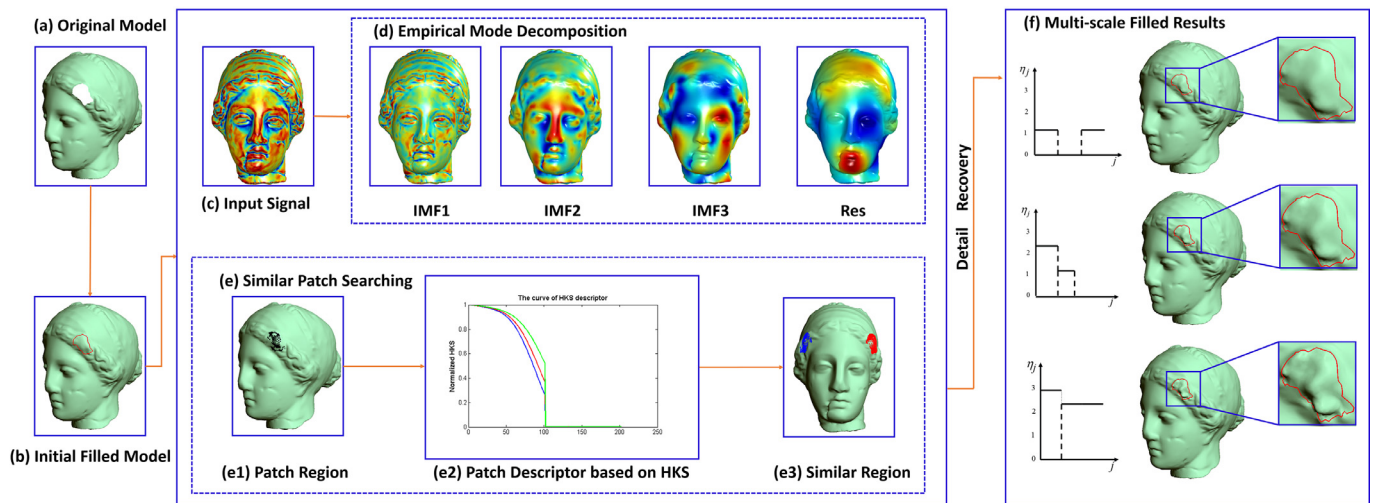
Fig. 1. The pipeline of EMD-based multi-scale detail recovery algorithm. (a) An original incomplete model. (b) An initial completed model with hole's boundary marked in red color. (c) The input signal defined by a measure of mean curvature. (d) EMD with the obtained IMFs and the residue. (e) Similar patch searching using patch descriptor constructed from HKS. (e.1) is the patch region and (e.2) is the HKS-based patch descriptor. (e.3) is the found similar region shown in blue color corresponding to the hole region in red. (f) Our multi-scale detail recovery results with different parameter settings. (For interpretation of the references to color in this figure legend, the reader is referred to the web version of this article).

try details, beyond the simple task of hole completion. In the literature, some texture synthesis-based methods [11,26,27], example-based [28] or template-based methods [29–33] or context-based methods [34–36] attempt to recover the missing shape and appearance of 3D surfaces. These methods usually cut the similar patch and paste them onto the hole region, and need to align, orient the patch with the hole boundary, which are complex in general. Moreover, in many cases, it is hard to accurately estimate the missing shapes in the hole region, the cut-and-paste operation merely produces a single and simple result, which limits the flexibility of hole-filling algorithms.

Focusing on geometry detail recovery with a goal of overcoming the above-mentioned limitations in mind, we devise a novel multi-scale geometry detail recovery algorithm for 3D surfaces based on Empirical Mode Decomposition (EMD). Different to the multi-scale representation algorithm in [37,38], EMD is a fully adaptive, data-driven algorithm, and works well for non-linear and non-stationary signal analysis and processing [39]. It decomposes the signal into a number of intrinsic mode functions (IMFs) and a residue, which encode the multi-level finer-scale details and the overall shape of the signal, respectively. In recent years, EMD has been successfully extended to 3D surface analysis and processing [40–45]. The elegant mathematical properties and the powerful multi-scale geometry detail representation of EMD strongly motivate us to expand EMD horizon in order to tackle new challenges in novel applications such as geometry detail recovery.

To fully recover the missing geometry details, we initially fill the hole region with a smooth completion serving as our baseline, and then search the most similar region corresponding to a larger region containing the initially-completed hole region. The searching process is based on patch descriptor constructed by Heat Kernel Signature(HKS) [46], which has a powerful geometric interpretation ability and captures much of the structure of the surface. Finally, benefiting from the multi-scale representation scheme, the desirable geometry details are transferred from the most similar region to the initially-completed region individually or in a combined manner. In contrast to the traditional hole-filling algorithms, our method is more flexible and can achieve versatile detail recovery results by selectively transferring geometry details at will. The pipeline of our multi-scale hole-filling algorithm is shown in Fig. 1 and the main contributions can be summarized as follows:

- *Automatic:* We propose an automatic multi-scale geometry detail recovery algorithm on 3D surfaces based on EMD. Our method does not rely on user interactions to specify the similar region or manually adding extra constraints for recovering the missing shapes, which enables our method to be effective and robust.
- *Flexible:* Unlike context-based or example-based methods, where the cut-and-paste operation is frequently employed, and complex cutting, stitching, gluing with surrounding surface are involved. Our method directly recovers the missing shapes via geometry detail transferring within the framework of EMD, which is much simpler and more flexible.
- *Versatile:* Different from traditional hole-filling algorithms, with which the holes are filled by smooth patches or less meaningful geometry shapes are obtained. Our method not only can effectively restore missing geometry details, but also can generate various meaningful filling results only made possible by the multi-level finer-detail representation of EMD, which enables our algorithm to be more versatile.

2. Related work

Considering that this paper focuses on geometry detail recovery on 3D surfaces, the most related works are briefly reviewed in this section, and for more works readers could refer to the survey of this subject [47,48].

Texture synthesis-based methods: To recover the missing geometry details, inspired by image completion algorithms, some texture synthesis-based methods have been proposed. Nguyen et al. [11] proposed a geometry completion and detail generation method by texture synthesis, which transforms the 3D geometry synthesis problem into 2D case by parameterizing surfaces and solves this problem in a 2D domain based on geometry gradient image. The final completed model can be reconstructed from synthesized local gradient image. Using gradient image to represent geometry details in a parameterization domain, the similar framework is also adopted in [27] by combining interactive user sketches to recover the structures and geometry details on 3D surfaces. In this process, parameterization is an important step. Even though the distortion in parameterizations during texture synthesis has been considered, the filling result could still be negatively

affected by severe distortion when dealing with shapes with high curvature. Breckon and Fisher [26] proposed a surface completion method by combining global surface fitting to derive an initial underlying geometric surface completion, with a 3D extension of nonparametric texture synthesis to provide the propagation of localized structural 3D surface details.

Example-based methods: Apart from texture synthesis based methods, another category of geometry recovery methods is example-based [28] or template-based [30]. These methods usually iteratively fill a hole by copying similar matching patches from other regions, or computing a mapping between the incomplete mesh with the template, then completing holes by cut-and-paste operation.

Using 3D shapes of database to provide geometric priors for regions of missing surface, Pauly et al. [28] proposed an example-based 3D scan completion algorithm. The method first retrieves suitable context models from the database, warps the retrieved models to conform with the incomplete data, and then consistently blends the warped models to obtain the final filled 3D shapes. Kraevoy and Sheffer [30] introduced a template-based mesh completion method by mapping the incomplete mesh with a template model. The template-based mesh completion can be viewed as mesh merging, which needs to merge the incomplete mesh with completing parts from the template. The main difficulty of merging operator in template-based completion is to accurate align the boundaries of holes with the template.

Integrating symmetry detection and surface matching, Li et al. [31] developed an iterative completion algorithm for completion of damaged skulls, which is further improved in [32] by employing a scale-space representation of shape based on heat kernel. Enlarging the database of template, Sung et al. [33] proposed a data-driven structural priors for shape completion, in which a collection of 3D shape examples are used to build structural part-based priors to complete holes.

Context-based methods: By analyzing the context of the given surface, Sharf et al. [34] introduced a context-based method, in which the characteristics of the given surface are first analyzed, then the hole is iteratively filled by copying patches from valid regions of the given surface. During this process, an initial octree is constructed, for each invalid surface cell, import and paste the content of valid surface cell from the well-aligned best matching patches with the surrounding surface by applying a rigid transformation. The method is limited by the relation between the sampling density and the detail frequency. To capture fine structural details, the cell must be small enough with respect to the detail size, which is very time-consuming.

Park et al. [35] developed a surface content completion method for repairing both shape and appearance of incomplete point clouds, which involves patch comparison based on local parameterization, computation of digital signature for patches, identification of the most resembling patch and final hole-filling via the cut-and-paste operation. Similar to most previous work, Harary et al. [36] proposed a context-based coherent surface completion algorithm, which filled the hole by synthesizing geometry shape from the found similar patches of the input mesh.

3. New algorithm

In this section, we first give an overview of our algorithm, and then introduce the algorithm in details, including EMD on 3D surfaces, similar patch identification, and geometry detail reconstruction.

3.1. Algorithmic overview

Given an incomplete surface $\mathbf{S} = (\mathbf{V}, \mathbf{F})$, where $\mathbf{V}$ represents a set of vertices $\mathbf{v}_i = (x_i, y_i, z_i) \in R^3$, $i = 1, \ldots, n$, and $\mathbf{F}$ contains connectivity information of the mesh including edges and faces. Our goal is to repair holes to obtain a complete model and recover geometry details. Fig. 1 shows the pipeline of our algorithm in the case of Igea model. For an incomplete model (Fig. 1(a)), we first fill the hole with an initial smooth surface to obtain an overall shape completion (Fig. 1(b)), which will serve as the base surface in the following steps. Then, we encode the geometry details by a measure of mean curvature (Fig. 1(c)) and use it as the input signal of EMD. The signal can be decomposed into a number of IMFs together with a residue, and represented in the multi-scale manner (Fig. 1(d)). After that, the most similar patch corresponding to each patch in the initially-filled region is searched based on the heat kernel signature (HKS) (Fig. 1(e)). To this point, the geometry details in the form of IMFs can be transferred from the most similar region to the initially-filled base surface. Finally, we can effectively reconstruct the missing geometry details from the new transferred signal (Fig. 1(f)). The algorithmic overview is documented in Algorithm 1.

Algorithm 1 Multi-scale geometry detail recovery.

Input: Incomplete surface $\mathbf{S}$

Output: Completed surface $\mathbf{S}$ with detail recovery

1: Initial smooth completion of $\mathbf{S}$ to obtain $\mathbf{S}'$ (Section 3.2)
2: Encode geometry details of the initially-completed surface $\mathbf{S}'$ by a measure of mean curvature and decompose the signal of surface $\mathbf{S}'$ into IMFs and a residue based on EMD (Section 3.3)
3: Search for the most similar patch from $\mathbf{S}$ for each target patch in the initially-filled region of $\mathbf{S}'$ (Section 3.4)
4: Transform the corresponding most similar patch's multi-scale geometrical details in the form of IMFs to the target patch to obtain the new signal (Section 3.5)
5: Reconstruct final geometry details from the new signal (Section 3.5.2)

3.2. Initial smooth surface completion

Before geometry detail recovery, the incomplete surface should be filled to obtain an initial smooth completion, which serves as a base surface for geometry detail recovery and provides a general appearance of geometry shape. In this work, we adopt the advancing front method used in [15,22] to obtain the initial filling result. If there are degenerated triangles or badly oriented triangles along the hole boundary, the method used in [14] will be adopted to recursively deleted them to prevent some undesired undulations or self-intersection in hole-filling. Fig. 1(b) shows the initial completion result of Fig. 1(a). For a given incomplete surface and an initial smoothly-filled surface, we shall endeavor our best efforts to recover geometry details as natural as possible in the following sections.

3.3. EMD on 3D surfaces

After obtaining the initial completion of surface, we represent the geometry details of the surface by using EMD, which is a powerful tool for processing non-linear and non-stationary signal and has been successfully extended to 3D surface analysis and processing [40–45]. For a given signal defined on 3D surface, EMD can represent the signal in a multi-scale manner and decompose the signal into a number of IMFs and a residue, which usually repre-

sent the multi-level finer-scale details and the overall shape of the signal.

For signal definition, the geometry coordinate components are used in [41]. However, the surface with different poses will result in different extrema of coordinate functions and further lead to different decomposition results, thus the signal of geometry coordinate is pose-dependent for EMD. To overcome this limitation, Hu et al. [42] used a measure of mean curvature as the input signal of EMD, which is both rotation-invariant and translation-invariant. This signal $\mathbf{f}$ can be computed by the inner product of Laplacian vector and the vertex's normal

$$\mathbf{f}(\mathbf{v}_i) = \mathbf{n}(\mathbf{v}_i) \cdot \delta(\mathbf{v}_i), \tag{1}$$

where $\mathbf{n}(\mathbf{v}_i)$ is the normal of vertex $\mathbf{v}_i$ and δ is the Laplacian operator on 3D surface

$$\delta(\mathbf{v}_i) = \sum_{j \in N(i)} w_{ij}(\mathbf{v}_j - \mathbf{v}_i), \tag{2}$$

with the cotangent weights

$$w_{ij} = cot\alpha_{ij} + cot\beta_{ij}, \tag{3}$$

where $N(i)$ is the vertex set of the 1-ring neighbors for vertex $\mathbf{v}_i$, and α_{ij}, β_{ij} are the angles opposite to the mesh edge (i, j).

The signal can be regarded as a measure of mean curvature, and it is both rotation and translation invariant. Therefore, we adopt this measure as the input signal of EMD, and then decompose it into a finite number of IMFs, which should satisfy the following conditions [39]

- In the whole data set, the number of extrema and the number of zero crossings must either equal or differ at most by one.
- At any point, the mean value of the envelope defined by the local maxima and the envelope defined by the local minima is zero.

IMFs are extracted from the input signal by the sifting process and leaving the final residue as constant or monotone trend. Specifically, the signal $\mathbf{f}$ about the measure of mean curvature can be decomposed and represented in a multi-scale manner

$$\mathbf{f} = \sum_{j=1}^{J} \mathbf{I}_j + \mathbf{r}_J, \tag{4}$$

where $\mathbf{I}_j, j = 1, \ldots, J$, $\mathbf{r}_J$ are IMFs and the residue (J is the number of IMFs), which represent the fine-scale details and a trend of signal. For the mean curvature signal used in the algorithm, the extracted IMFs are called MC-IMFs (mean curvature IMFs) in this paper.

The entire process of EMD is summarized in Algorithm 2 and more details of the EMD algorithm can refer to [41,42]. Fig. 2 shows the decomposition results of a signal defined on a bunny model. To visualize MC-IMFs and the residue, the models corresponding to MC-IMFs and the residue are reconstructed using its MC-IMFs together with the residue. From the reconstruction results, we can see that geometry details are encoded in the leading MC-IMFs, and the smoother shape is contained in the residue.

3.4. Searching for similar patches

To this point, we have obtained the multi-scale geometry detail representation. For geometry detail recovery we need to decide which region of geometry details will be transferred to the smooth filled region. In this paper, the Heat Kernel Signature (HKS) [46] based algorithm is adopted to search for the most similar region in the initially-filled surface.

Algorithm 2 3D EMD algorithm on surfaces.

Input: A signal $\mathbf{f}$ computed from the surface $\mathbf{S}$
Initialization: Set the initial residue as $\mathbf{r}_0 = \mathbf{f}$ and $j = 1$ for the initial index of IMFs;
    repeat
2:    $\mathbf{t}_0 = \mathbf{r}_{j-1}, k = 1$;
    for each k **do**
4:    Detect all local minima and local maxima of the signal $\mathbf{t}_{k-1}$;
    According to biharmonic interpolation, the lower envelope $\mathbf{Lt}_{k-1}$ (upper envelope $\mathbf{Ut}_{k-1}$) can be obtained by interpolating all local minimal (local maximum);
6:    Compute the mean envelope $\mathbf{Mt}_{k-1}$ of $\mathbf{t}_{k-1}$ by $\mathbf{Mt}_{k-1} = (\mathbf{Lt}_{k-1} + \mathbf{Ut}_{k-1})/2$;
    Update $\mathbf{t}_k = \mathbf{t}_{k-1} - \mathbf{Mt}_{k-1}$;
8:    **if** $\mathbf{t}_k$ satisfiesthe stopping criterion **then**
    Obtain the $j - th$ IMF $\mathbf{I}_j = \mathbf{t}_j$ and the $j - th$ residue $\mathbf{r}_j = \mathbf{r}_{j-1} - \mathbf{I}_j$;
10:    $j = j + 1$;
    break;
12:    **else**
    $k = k + 1$;
14:    **end if**
    end for
16: **until** The residue is a constant or monotonic function
Output: IMFs $\mathbf{I}_j, j = 1, \ldots, J$ and a residue $\mathbf{r}_J$

3.4.1. Descriptor definition

HKS is a powerful descriptor for characterizing local and global geometry of the surface patch centered at each vertex [32,46]

$$h_t(x) = \sum_{i=0}^{\infty} e^{-\lambda_i t} \Omega_i(x)^2, \tag{5}$$

where λ_i is the eigenvalue and Ω_i is the corresponding eigenfunction of the Laplace–Beltrami operator. Fig. 3 shows the HKS curves for three different types of vertices, in which they are well distinguished from each other. Fig. 4 shows HKS curves of the same vertex on three different cases. The first case is the original model with the target vertex marked in blue color. The second case is the model with the target vertex locating on the hole boundary and marked in red color. The third case is the initial filled model with the target vertex marked in green color. The HKS curves of them are shown in the middle. From the curves, we can see that blue curve almost coincides with the green curve, while both of them deviate from the red curve. Two conclusions can be obtained, the first one is that computing the HKS on the initial filled model is much better than directly computing the HKS on the incomplete model. The second one is that it is reasonable to compute the HKS (in part) over the smooth filling, which does not bias the descriptor in a negative way though there is an initial filled smooth part.

The value of *HKS* over different times can be regarded as the signature of vertex and provide an effective multi-scale signature for shape matching. However, *HKS* on one vertex is not enough to character the similarity of patches, which can be defined as the connected neighborhood that is falling within a ball of radius r_1 centered at $\mathbf{v}_i$. Therefore, we adopt the statistical information of the *HKS* to define patch descriptor [36]

$$HKS(p_i) = \{HKS_\mu(p_i)_{[0,1]}, HKS_{\sigma^2}(p_i)_{[0,1]}\}, \tag{6}$$

where the symbol [0,1] means normalizing the value of *HKS* to [0,1].

The above descriptor contains two components. The first one is the average of the *HKS* values of the patch's vertices, which is performed at each time t of the *HKS* and denoted as HKS_μ. An-
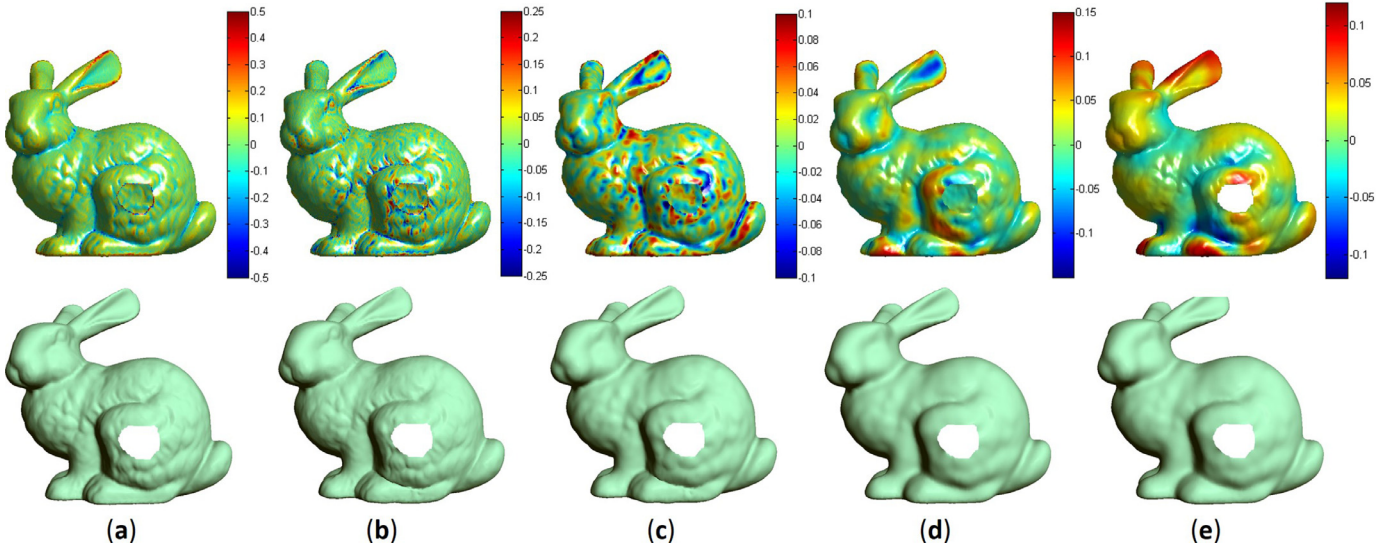
Fig. 2. The EMD decomposition results of Bunny model. (a) Original model with the input signal. (b–d) The first three MC-IMFs and the corresponding reconstruction results from MC-IMFs together with the residue. (e) The reconstruction result from the residue.
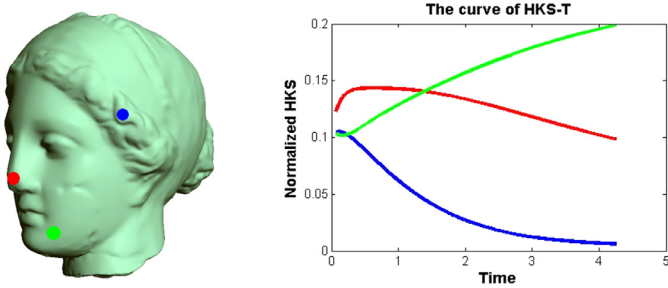
Fig. 3. Discriminative power of *HKS*. Left: Three vertices of Igea mode are marked in blue, red, and green, respectively. Right: The HKS values of three vertices are marked in corresponding colors. (For interpretation of the references to color in this figure legend, the reader is referred to the web version of this article).

Fig. 4. Robustness of the HKS. Left: The original model with target vertex marked in blue. Right: The model with hole locating on the hair region, and the target vertex is marked in red. Below: The initial completed model and the target vertex is marked in green. Middle: The HKS curves are marked in blue, red and green corresponding to the vertices marked in left, right and below model. (For interpretation of the references to color in this figure legend, the reader is referred to the web version of this article).

other one is the variance of these values and denoted as a vector of variances HKS_{σ^2}. In this work, three time domains are used: the entire time domain, the lower 3/4 and the lower half of the entire time domain. That is to say, there exists three descriptors for each patch. Following the suggestion of [46], the smaller 300 eigenvalues and corresponding eigenvectors are computed for each model, and we uniformly sample 100 vertices in the logarithmically scale over time interval $[4ln(10)/\lambda_{300}, 4ln(10)/\lambda_2]$.

3.4.2. Similar patch identification

For each target patch T_i in the initially-filled region of $\mathbf{S}'$, we search for k similar patches S_j from the original surface $\mathbf{S}$ as candidate patches. The patch can be defined as the connected neighborhood that is falling within a ball of radius r_1 around the current vertex $\mathbf{v}_i$. The default value of k is set to 0.1% of the whole number of vertices. In this paper, we adopt Euclidean distance to measure the similarity between two patches based on the well-defined patch descriptor. It should be pointed out that, the candidate's patches may be included in the initially-filled region, which should be removed to avoid extra calculations and misleading results. To achieve this, we restrict the candidate patches far from the current vertex with the radius r_2.

After finding all candidate patches for T_i, $S(T_i) \subset \mathbf{S}$, the most similar patch will be finally selected from them through a rigid alignment. The alignment is performed by finding matching points between source patch and target patch using *HKS*. Based on the

matching pairs, the rigid transformation $\mathbf{R}$ between T_i and $S_j \subset S(T_i)$ is calculated by solving a least-squares minimization

$$D(S_j, T_i) = \sum_{l=1}^{\#(T_i)} ||\mathbf{v}_l^{S_j} - (\mathbf{R} \cdot \mathbf{v}_l^{T_i} + \mathbf{t})||^2, \qquad (7)$$

where $\mathbf{v}_l^{T_i}$ is a vertex of T_i, and $\mathbf{v}_l^{S_j}$ is the matching vertex in S_j, $\#(T_i)$ is the number of vertex in patch T_i, $\mathbf{R}$ is a rotation matrix and $\mathbf{t}$ is a translation vector. Eq. (7) can be solved by using the shape matching method proposed in [49]. Finally, for each target patch, the source patch with the smallest error will be selected as the most similar patch. Figs. 1(c) and 6(c) show the most similar region of the hole in hair of Igea model, respectively. As can be seen from these figures, the patch descriptor well describes the similarity between patches and leads to satisfactory results.
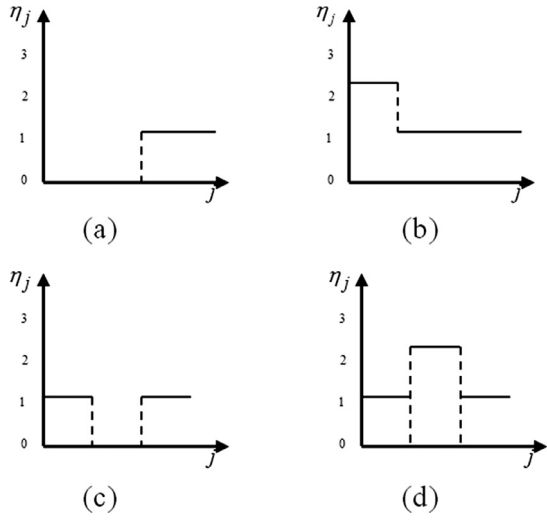
Fig. 5. Weight values η_j for multi-scale representation and editing. (a) Low-pass filtering. (b) High-enhancement filtering. (c) Band-stop filtering. (d) Band-enhancement filtering.
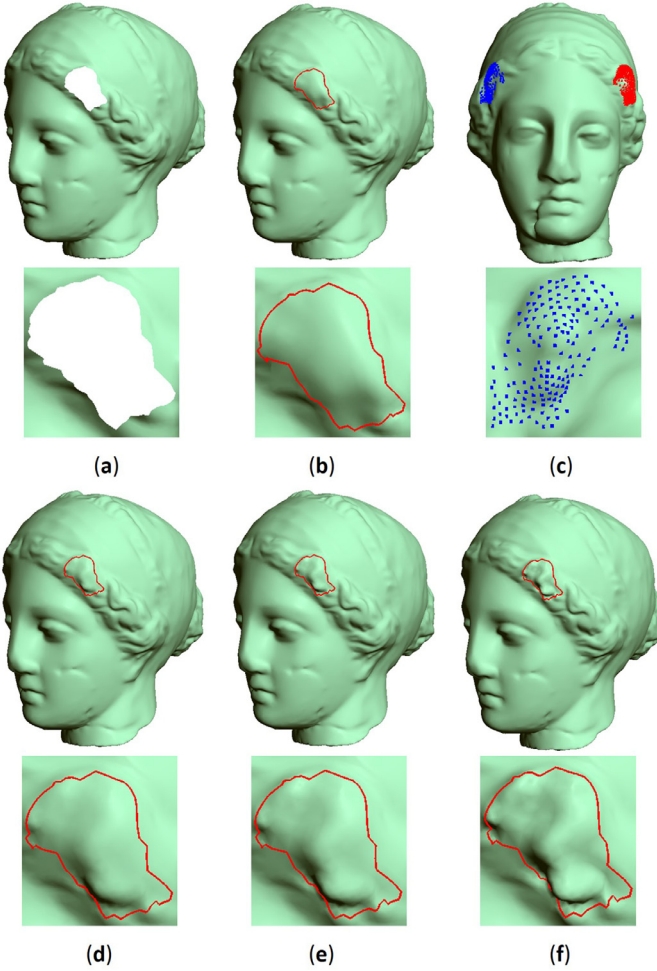
Fig. 6. Multi-scale detail recovery results on Igea model. (a) The incomplete model. (b) The initial completed result. (c) The most similar region is selected by *HKS* and the blue region is the most similar region of the red region, which is composed of the center vertices of all the most similar patches. (d–f) The multi-scale hole-filling results with details using our method. The η_j of the MC-IMFs are (1,0,1), (2,1,0), (3,2,1), respectively. (For interpretation of the references to color in this figure legend, the reader is referred to the web version of this article).

3.5. Multi-scale geometry detail recovery

In the literature, most previous work [11,26–36] adopt the copy-and-paste operation to recover the missing geometry details. However, these methods can only produce single filling result, and limit the flexibility of the algorithm to a large extent. In contrast, we develop a novel multi-scale geometry detail recovery algorithm within the framework of EMD, which is more flexible and powerful than previous work.

3.5.1. Detail transfer

According to Eq. (4), the signal $\mathbf{f}$ defined on initially-filled surface S' can be expressed in multi-scale representation and for each vertex $\mathbf{v}_i$, we have

$$\mathbf{f}(\mathbf{v}_i) = \sum_{j=1}^{J} \mathbf{I}_j(\mathbf{v}_i) + \mathbf{r}_J(\mathbf{v}_i), \tag{8}$$

where $\mathbf{I}_j (j = 1, \ldots, J)$ and $\mathbf{r}_J$ are the corresponding MC-IMFs and the residue.

For each vertex $\mathbf{v}_i$ in the initially-filled region, there are several patches containing vertex $\mathbf{v}_i$. Each patch containing $\mathbf{v}_i$ will find a most similar patch. Then, the center of the most similar patch for each vertex $\mathbf{v}_i$ is used to represent the similar region corresponding to the initially-filled region. Therefore, there are a set of most similar patches corresponding to the patches containing vertex $\mathbf{v}_i$. For each of them, we can find the closest vertex on the aligned source patch using rigid alignment. Denote all closest vertices in all most similar patches as $C(\mathbf{v}_i)$, the geometry details encoded in MC-IMFs of $C(\mathbf{v}_i)$ can be collected to compute the new signal value of vertex $\mathbf{v}_i$

$$\mathbf{I}'_j(\mathbf{v}_i) = \frac{1}{n_c} \sum_{\mathbf{v}_l \in C(\mathbf{v}_i)} \mathbf{I}^S_j(\mathbf{v}_l), \tag{9}$$

where n_c is the number of corresponding points set $C(\mathbf{v}_i)$, and $\mathbf{I}^S_j$ is the j-th MC-IMF of the source patch.

To this point, we have established the correspondence between the source patch and the initially-filled region, therefore, replacing part of signal in the initially-filled region by the newly-assigned values computed in Eq. (9), we obtain the new signal $\tilde{\mathbf{f}}$

$$\tilde{\mathbf{f}}(\mathbf{v}_i) = \sum_{j=1}^{J} \frac{1}{n_c} \sum_{\mathbf{v}_l \in C(\mathbf{v}_i)} \mathbf{I}^S_j(\mathbf{v}_l) + \mathbf{r}_J(\mathbf{v}_i), \tag{10}$$

in which the residue of signal defined on the initially-filled region is retained to preserve the overall shape of the initially-filled surface.

3.5.2. Surface reconstruction

Our geometry detail recovery is only achieved within the framework of signal processing based on EMD, therefore, the final shape of filled region can be reconstructed from the modified signals after geometry detail transfer. With the new signal $\tilde{\mathbf{f}}$, the recovery geometry shapes with vertices $\tilde{\mathbf{V}}$ can be reconstructed by minimizing the following energy formulation

$$\|\mathbf{L}\tilde{\mathbf{V}} - diag(\tilde{\mathbf{f}})\mathbf{N}\|^2 + \lambda^2 \sum_{i=1}^{\tilde{n}} \|\tilde{\mathbf{v}}_i - \mathbf{v}_i\|^2, \tag{11}$$

with the weighting factor λ for the positions of initially-filled surface serving as constraints, and the default value is set to be 0.1 in our experiments. $\tilde{n}$ is the number of vertices in initially-filled surface. $\mathbf{N}$ is the normal matrix of vertices and $\mathbf{L}$ is the Laplacian matrix with elements of

$$\mathbf{L}_{ij} = \begin{cases} \sum_{j \in N(i)} w_{ij}, & if \quad i = j \\ -w_{ij}, & if \quad j \in N(i), \\ 0, & otherwise \end{cases} \quad (12)$$

where $N(i)$ is the vertex set of 1-ring neighbors of $\mathbf{v}_i$ and w_{ij} is the weight defined by $w_{ij} = \cot \alpha_{ij} + \cot \beta_{ij}$, $\cot \alpha_{ij}$ and $\cot \beta_{ij}$ are the angles opposite to edge (i, j).

3.5.3. Versatile geometry detail recovery

As mentioned in the above sections, EMD can decompose a signal into a number of MC-IMFs and a residue, where the leading MC-IMFs encode the fine-scale details and the residue represents the overall shape of signal. Therefore, it is natural to achieve multi-scale geometry detail recovery by scaling corresponding MC-IMFs with residue unchanged. Specifically, adjustable weights η_j can be integrated into Eq. (10) to produce multi-scale recovery results

$$\tilde{\mathbf{f}}(\mathbf{v}_i) = \sum_{j=1}^{J} \eta_j \frac{1}{n_c} \sum_{\mathbf{v}_l \in C(\mathbf{v}_i)} \mathbf{I}_j^S(\mathbf{v}_l) + \mathbf{r}_J(\mathbf{v}_i). \quad (13)$$

Therefore, we can recover the geometrical details while editing them according to specific requirements simultaneously by adjusting the weight η_j. The transferred details corresponding to j-th MC-IMF will be enhanced if $\eta_j > 1$, and will be smoothed if $\eta_j < 1$. Fig. 5 shows the different setting of η_j, including low-pass filtering, high-enhancement filtering, band-stop filtering, and band-enhancement filtering, respectively. Through setting the different values of η_j we can achieve multi-scale geometry detail recovery results (see Fig. 1(f)).

Fig. 6 shows the procedure of geometry detail recovery based on multi-scale representation of EMD. Fig. 6(a) is the Igea model with the missing shape on the region of hair. The shape and appearance of the missing part of the hair will be completed with details taking from the similar region. Fig. 6(b) shows the initial smoothly-filled result, which serves as the base surface in following steps. Benefiting from the HKS-based patch descriptor, the most similar region with the hole can be easily identified. Fig. 6(c) shows the most similar region located in the region of right head marked in red color. Under the signal processing framework of EMD, the geometry details of the most similar region are transferred to the smooth base surface, and we can obtain our final geometry detail recovery results. From Fig. 6(d)–(f), we can see that the details of hair are gradually appearing and becoming much clearer with the increasing weights of MC-IMFs.

4. Experimental results and discussions

To illustrate the effectiveness of our algorithm towards recovering complex geometry details, a large number of experimental results are shown in this section. We also compare our algorithm with previous algorithms to show the advantages of our method. Before demonstrating the results, we first discuss the parameters used in the algorithm, and then show the experimental results.

4.1. Parameters and performance

We have implemented the proposed geometry detail recovery algorithm in Matlab2013a on a Laptop with the Intel Core i7-4790 CPU @ 3.60 GHz with 16.0 GB memory. The parameters r_1 and r_2 are both the radii of patches, in which r_1 is used in patch descriptor and r_2 is used in similar patch identification. The parameter r_1 is chosen differently for different models, which determines the size of target patches in the initially-filled region and the similar patches S_j from the original surface. The size of the patches should not be too large or too small. Larger patches will increase the amount of computation, while smaller patches cannot characterize the similarity of different patches. In our experiment, this

Table 1
Run times (in seconds). #(V): number of vertices. #(FV): number of filled vertices. r_1: radius of patch. r_2: radius of hole to prevent the influence of hole. They are all set as several times of the average length of mesh edges. EMD: time of EMD applied on the signal of 3D surface. FSP: time of most similar patch searching. Total: total time of our method.

Figs	#(V)	#(FV)	r_1	r_2	EMD	FSP	Total
Fig. 6	26,635	295	4	8	10.550	51.906	99.969
Fig. 7	48,961	445	5.5	11	26.222	214.804	248.348
Fig. 8	25,220	101	4	8	11.453	26.043	41.665
Fig. 9	34,142	153	4	8	15.229	42.721	63.501
Fig. 10	34,539	581	5.5	11	43.549	155.138	203.924
Fig. 11	96,431	42	2.5	5	41.826	54.959	109.70
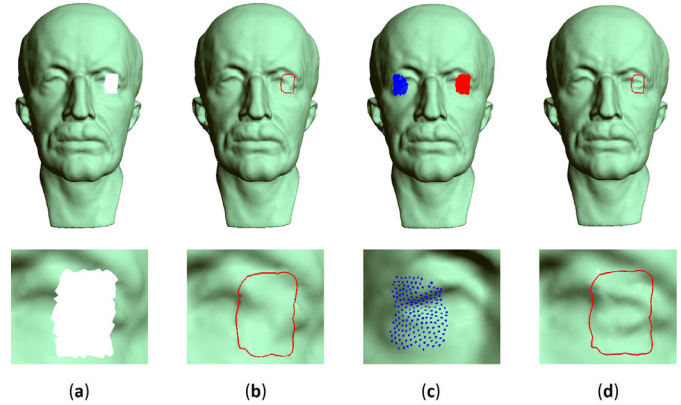
Fig. 7. Hole-filling result on Maxplank model. (a) Incomplete model. (b) Initial completed result. (c) Most similar region of the red region is shown in blue, which is composed of the center vertices of all the most similar patches. (d) Hole-filling result of our method. The η_j of the MC-IMFs is (1,1,1). (For interpretation of the references to color in this figure legend, the reader is referred to the web version of this article).

parameter is chosen empirically and is usually set by several times of the average length of mesh edges. The main factor affecting this parameter is the sparsity of the mesh. For a density mesh, the length of mesh edge will be small, to obtain a proper size of patch, a larger r_1 will be set. In contrast, for a sparse mesh, a smaller value will be used. Usually, radius r_2 should be larger than r_1, and $r_2 = 2 * r_1$ will be used in all of our experiments. In signal decomposition, more MC-IMFs could provide more flexibility for the algorithm, however, it also takes more time. To seek a trade-off between the flexibility and the efficiency of the algorithm, the number of MC-IMFs is set to three as a default value. The running time mainly depends on the size of the model, the size of the patch, and the size of the hole. The most time-consuming part is the similar patch identification with the global searching strategy. Table 1 shows the parameters and the running time of the models used in our experiments.

4.2. Application examples and comparisons

Fig. 7 shows the detail recovery results on a Maxplank model. For the model with a hole on left eye (see Fig. 7(a)), we first get an initial smooth completion as the base surface (see Fig. 7(b)). Based on the initial completion, we apply EMD on the similar region (Fig. 7(c)) found by the HKS-based patch descriptor to obtain the multi-scale detail representation. For the intrinsic symmetry structure of Manxplank model, our similar patch searching strategy can accurately find the most similar region on the right eye. Then, we can easily achieve the detail recovery by transferring and adjusting the weights of corresponding MC-IMFs. From Fig. 7(d), we can see that the missing shape in the region of eye is effectively recovered as well as the textures of eyebrow.
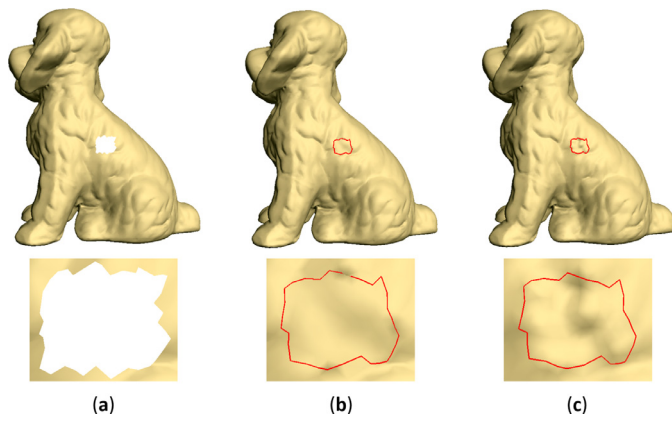
Fig. 8. Hole-filling result on Dog model. (a) The incomplete model. (b) The initial completed result. (c) The hole-filling result of our method. The η_j of the MC-IMFs is (5,4,4).
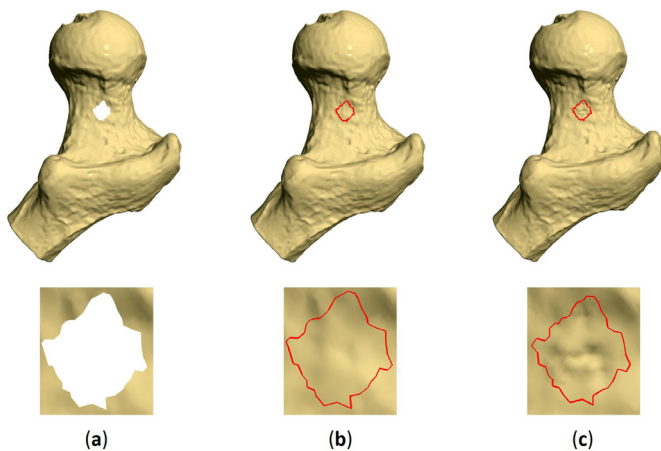
Fig. 9. Hole-filling result on noisy Balljoint model. (a) The incomplete model. (b) The initial completed result. (c) The hole-filling results of our method. The η_j of the MC-IMFs is (3,3,3).

Fig. 8 shows the result of our method on a detail-rich dog model. Fig. 8(b) is the smoothly-filled result, and the final filled result shown in Fig. 8(c). From the result we can see that the hole is well filled with detail recovery. Furthermore, our algorithm can also obtain satisfactory filling result for incomplete model with noise. Fig. 9 shows the hole-filling result on the noisy balljoint model. Fig. 9(a) is the incomplete mode contaminated with heavy noises. Fig. 9(b) is the initial filling result and Fig. 9(c) is the result obtained by our method, in which the geometry details are well recovered.

Benefiting from the multi-scale decomposition of signal, our hole-filling algorithm can be executed in a multi-scale manner and produce versatile filling results. Apart from the multi-scale recovery results shown in Fig. 6, a shape completion on the left leg of bunny model with multi-scale context control is further illustrated in Fig. 10. Fig. 10(b) is the initial smooth completion and Fig. 10(c) is the most similar patch found from another region of leg and is shown in blue color. The geometry details of the most similar patch are transferred to smoothly-filled region within the framework of EMD. With the increasing weights of leading MC-IMFs, the geometry details are gradually presented, and multi-scale geometry detail recovery results are obtained (see Fig. 10(d–f)).

In Figs. 11 and 12, to illustrate the efficiency of our hole-filling algorithm, we compare our algorithm with previous algorithms and softwares, including MeshFix algorithm [20], the software of MeshLab [9], radial basis function (RBF) algorithm [50], Polymender algorithm [51] and RameshCleaner algorithm [52].

Fig. 11 shows the comparison results with these methods on the armadillo model with a hole on the waist region in Fig. 11(a). Fig. 11(b) is the result of MeshFix algorithm, which fills the hole by the patching procedure and fails to recover the geometry details of the missing region. The result of Fig. 11(c) is obtained by the software of MeshLab, which also does not produce satisfactory filling results. Fig. 11(d) demonstrates the result of the RBF method, which utilizes the RBF algorithm to interpolate vertices around missing regions. Fig. 11(e) illustrates the result of Polymender software and Fig. 11(f) is the result of RameshCleaner algorithm. From these results, we can see that Fig. 11(b) and (d) results are better than others and achieve smooth transition between the original model with the filled patch. Although all of the above algorithms could obtain the completed results, the geometry details on the waist are still not well recovered. Comparing with these results, Fig. 11(g) shows our filling result, which not only can obtain smooth transition across the surrounding boundary between the filling patch and adjacent region, but also produce the satisfactory result with the proper recovery of missing geometry details.

Fig. 12 shows the hole-filling results of bunny model with the missing shape in the leg region. The results shown in Fig. 12(b–f) are obtained by the algorithms of MeshFix [20], MeshLab [9], RBF [50], Polymender [51], and RameshCleaner [52], respectively. From the results, we can observe that the methods of MeshFix and RBF produce more smooth results than other methods. On the other hand, the results obtained by MeshLab, Ploymender, and Ramesh-Cleaner have some artifacts in the transition regions connecting the filled patch and the existing geometry outside the hole region. More importantly, the missing geometry details are not well restored in other methods. In contrast, with the most similar region being properly identified (aided by our shape descriptor) and the multi-scale representation enabled by the EMD of shape geometry, our algorithm produces more pleasing result than that from other algorithms and could effectively recover the missing geometry details (see Fig. 12(g)).

4.3. Limitation and future work

As discussed above in this section, there are many types of missing data, we are only focusing on geometry detail recovery on 3D surfaces in this paper. Therefore, our method might not work well for the model with missing sharp features. Another limitation is that, our algorithm is based on similar patch search and identification, which could be time-consuming for large-sized models due to the global searching strategy being adopted. To overcome these limitations, we would like to integrate the functionality of sharp feature recovery into our current data completion framework in the near future. And the parallel computation, kd-based searching algorithm may be adopted to accelerate the similar patch searching.

Furthermore, for large holes, due to the behaviors of HKS would be very different on meshes, the most similar region could not be searched in an accurate way, which will lead to unsatisfactory filling results. In this situation, just searching the similar patch from itself is inadequate. Searching in a large collection of 3D models and resorting to some powerful techniques, such as deep learning, may provide good solutions for the hole-filling of meshes with large holes.

5. Conclusion

In this paper, we have developed a multi-scale EMD-based geometry detail recovery algorithm for incomplete surfaces. Our method first fills the missing region with a smooth patch to establish a base surface, and the most similar region is elaborately searched based on shape descriptor constructed from heat kernel
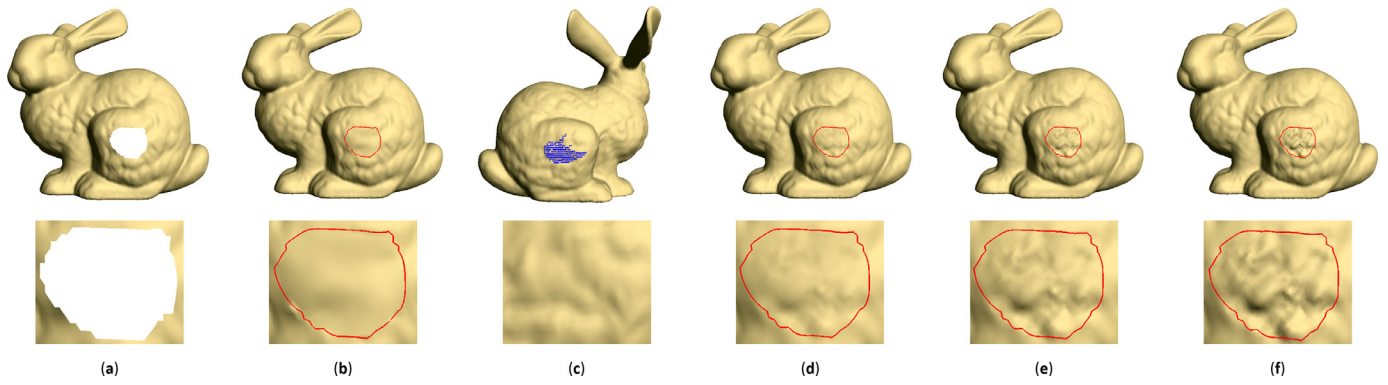
Fig. 10. Multi-scale detail recovery results on Bunny model. (a) The incomplete model. (b) The initial completed result. (c) The most similar region is marked in blue, which is composed of the center vertices of all the most similar patches. (d–f) The multi-scale hole-filling results of our method. The η_j of the MC-IMFs are (1,0,1), (2,1,0), and (3,2,1), respectively. (For interpretation of the references to color in this figure legend, the reader is referred to the web version of this article).
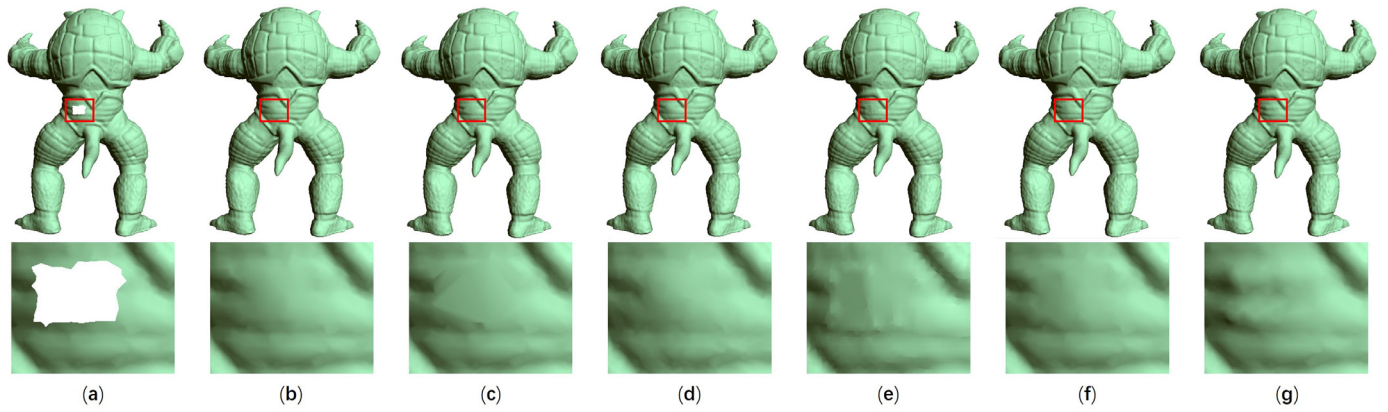
Fig. 11. Comparisons between our method and the previous hole-filling algorithms on Armadillo model. (a) The incomplete model. (b) The result of MeshFix method [20]. (c) The result of Meshlab software filling method [9]. (d) The result of RBF [50]. (e) The result of Polymender [51]. (f) The result of RameshCleaner [52]. (g) The result of our method.
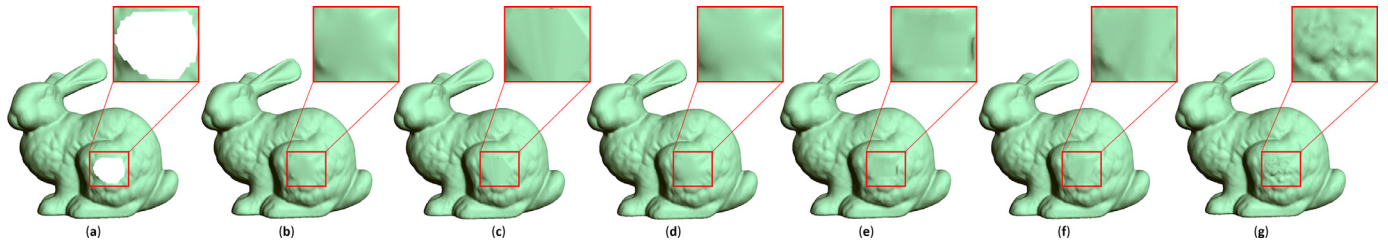
Fig. 12. Comparisons between our method and the previous hole-filling algorithms on Bunny model. (a) The incomplete model. (b) The result of MeshFix method [20]. (c) The result of Meshlab software filling method [9]. (d) The result of RBF [50]. (e) The result of Polymender [51]. (f) The result of RameshCleaner [52]. (g) The result of our method.

signature. Then, the geometry detail signals from the most similar region are transferred to the smoothly-filled patch based on the multi-scale representation of EMD. Finally, we can effectively reconstruct the missing geometry details from the transferred signal. Comparing with traditional methods (i.e., example-based or context-based methods), which usually resort to complex, and/or cut-and-copy operators, we develop a multi-scale geometry detail recovery algorithm based on EMD, which is effective and flexible, and can produce versatile detail recovery results. A large number of experiments and comparisons have been performed to demonstrate the effectiveness of our EMD-based multi-scale geometry detail recovery algorithm.

References

[1] Curless B, Levoy M. A volumetric method for building complex models from range images. In: Proceedings of the 23rd annual conference on computer graphics and interactive techniques; 1996. p. 303–12.

[2] Davis J, Marschner S, Carr M, Levoy M. Filling holes in complex surfaces using volumetric diffusion. In: Proceedings of the first international symposium on 3D data processing, visualization, and transmission; 2002. p. 428–38.

[3] Nooruddin FS, Turk G. Simplification and repair of polygonal models using volumetric techniques. IEEE Trans Vis Comput Graph 2003;9(2):191–205.

[4] Ju T. Robust repair of polygonal models. ACM Trans Graph 2004;23(3):888–95.

[5] Bischoff S, Kobbelt L. Structure preserving cad model repair. Comput Graph Forum 2005;24(3):527–36.

[6] Bischoff S, Pavic D, Kobbelt L. Automatic restoration of polygon models. ACM Trans Graph 2005;24(4):1332–52.

[7] Podolak J, Rusinkiewicz S. Atomic volumes for mesh completion. In: Proceedings of the third eurographics symposium on geometry processing, SGP '05; 2005. p. 31–41.

[8] Carr JC, Beatson RK, Cherrie JB, Mitchell TJ, Fright WR, McCallum BC. Reconstruction and representation of 3d objects with radial basis functions. In: Proceedings of the 28th annual conference on computer graphics and interactive techniques, SIGGRAPH '01; 2001. p. 67–76.

[9] Liepa P. Filling holes in meshes. In: Proceedings of the 2003 eurographics/ACM SIGGRAPH symposium on geometry processing, SGP '03; 2003. p. 200–5.

[10] Lévy B. Dual domain extrapolation. ACM Trans Graph 2003;22(3):364–9.

[11] Nguyen MX, Yuan X-R, Chen B-Q. Geometry completion and detail generation by texture synthesis. Vis Comput 2005;21(9–10):669–78.

[12] Jun Y. A piecewise hole filling algorithm in reverse engineering. Comput Aided Des 2005;37(2):263–70.

[13] Bendels GH, Schnabel R, Klein R. Detail-preserving surface inpainting. In: Proceedings of the 6th international symposium on virtual reality, archaeology and cultural heritage, VAST; 2005. p. 41–8.

[14] Pernot J-P, Moraru G, Véron P. Filling holes in meshes using a mechanical model to simulate the curvature variation minimization. Comput Graph 2006;30(6):892–902.

[15] Zhao W, Gao S-M, Lin H-W. A robust hole-filling algorithm for triangular mesh. Vis Comput 2007;23(12):987–97.

[16] Xiao C-X, Zheng W-T, Miao Y-W, Zhao Y, Peng Q-S. A unified method for appearance and geometry completion of point set surfaces. Vis Comput 2007;23(6):433–43.

[17] Chen C-Y, Cheng K-Y. A sharpness-dependent filter for recovering sharp features in repaired 3d mesh models. IEEE Trans Vis Comput Graph 2008;14(1):200–12.

[18] Brunton A, Wuhrer S, Shu C, Bose P, Demaine ED. Filling holes in triangular meshes by curve unfolding. In: Proceedings of IEEE international conference on shape modeling and applications, SMI; 2009. p. 66–72.

[19] Li Z, Meek DS, Walton DJ. Polynomial blending in a mesh hole-filling application. Comput Aided Des 2010;42(4):340–9.

[20] Attene M. A lightweight approach to repairing digitized polygon meshes. Vis Comput 2010;26(11):1393–406.

[21] Panchetti M, Pernot J-P, Véron P. Towards recovery of complex shapes in meshes using digital images for reverse engineering applications. Comput Aided Des 2010;42(8):693–707.

[22] Wang X, Liu X, Lu L, Li B, Cao J, Yin B, et al. Automatic hole-filling of cad models with feature-preserving. Comput Graph 2012;36(2):101–10.

[23] Harary G, Tal A, Grinspun E. Feature-preserving surface completion using four points. Comput Graph Forum 2014;33(5):45–54.

[24] Zhong M, Qin H. Surface inpainting with sparsity constraints. Comput Aided Geom Des 2016;41:23–35.

[25] Yang L, Yan Q, Xiao C. Shape-controllable geometry completion for point cloud models. Vis Comput 2016:1–14.

[26] Breckon TP, Fisher RB. Three-dimensional surface relief completion via nonparametric techniques. IEEE Trans Pattern Anal Mach Intell 2008;30(12):2249–55.

[27] Yang S, Qi Y, Qin H. Simultaneous structure and geometry detail completion based on interactive user sketches. Sci China Inf Sci 2012;55(5):1123–37.

[28] Pauly M, Mitra NJ, Giesen J, Gross M, Guibas LJ. Example-based 3d scan completion. In: Proceedings of the third eurographics symposium on geometry processing, SGP '05; 2005. p. 23–32.

[29] Anguelov D, Srinivasan P, Koller D, Thrun S, Rodgers J, Davis J. Scape: shape completion and animation of people. ACM Trans Graph 2005:408–16.

[30] Kraevoy V, Sheffer A. Template-based mesh completion. In: Proceedings of the third eurographics symposium on geometry processing, SGP '05; 2005. p. 13–22.

[31] Li X, Yin Z, Wei L, Wan S-H, Yu W, Li M-Q. Symmetry and template guided completion of damaged skulls. Comput Graph 2011;35(4):885–93.

[32] Yu W, Li M, Li X. Fragmented skull modeling using heat kernels. Graph Models 2012;74(4):140–51.

[33] Sung M, Kim VG, Angst R, Guibas L. Data-driven structural priors for shape completion. ACM Trans Graph 2015;34(6) 175:1–175:11.

[34] Sharf A, Alexa M, Cohen-Or D. Context-based surface completion. ACM Trans Graph 2004;23:878–87.

[35] Park S, Guo X-H, Shin H, Qin H. Surface completion for shape and appearance. Vis Comput 2006;22(3):168–80.

[36] Harary G, Tal A. Grinspun E. Context-based coherent surface completion. ACM Trans Graph 2014;33(1) 5:1–5:12.

[37] Pauly M, Kobbelt LP, Gross M. Point-based multiscale surface representation. ACM Trans Graph 2006;25(2):177–93.

[38] Nader G, Guennebaud G, Mellado N. Adaptive multi-scale analysis for point-based surface editing. Comput Graph Forum 2014;33(7):171–9.

[39] Huang NE, Shen Z, Long SR, Wu MC, Shih HH, Zheng Q, et al. The empirical mode decomposition and the hilbert spectrum for nonlinear and non-stationary time series analysis. Proc R Soc Lond Ser A: Math Phys Eng Sci 1998;454(1971):903–95.

[40] Qin X, Hong CX, Zhang SQ, Wang WH. Emd based fairing algorithm for mesh surface. In: Proceedings of CAD/Graphics '09.; 2009. p. 606–9.

[41] Wang H, Su Z, Cao J, Wang Y, Zhang H. Empirical mode decomposition on surfaces. Graph Models 2012;74(4):173–83.

[42] Hu J, Wang X, Qin H. Improved, feature-centric emd for 3d surface modeling and processing. Graph Models 2014;76(5):340–54.

[43] Wang X, Hu J, Zhang D, Qin H. Efficient emd and Hilbert spectra computation for 3d geometry processing and analysis via space-filling curve. Vis Comput 2015;31(6):1135–45.

[44] Hu J, Wang X, Qin H. Novel and efficient computation of hilbert huang transform on surfaces. Comput Aided Geom Des 2016;43:95–108.

[45] Zhang D, Wang X, Hu J, Qin H. Interactive modeling of complex geometric details based on empirical mode decomposition for multi-scale 3d shapes. Comput-Aided Des 2017;87:1–10.

[46] Sun J, Ovsjanikov M, Guibas L. A concise and provably informative multi-scale signature based on heat diffusion. Comput Graph Forum 2009;28(5):1383–92.

[47] Ju T. Fixing geometric errors on polygonal models: a survey. J Comput Sci Technol 2009;24(1):19–29.

[48] Attene M, Campen M, Kobbelt L. Polygon mesh repairing: an application perspective. ACM Comput Surv 2013;45(2):15–48.

[49] Müller M, Heidelberger B, Teschner M, Gross M. Meshless deformations based on shape matching. ACM Trans Graph 2005;24(3):471–8.

[50] Branch J, Prieto F, Boulanger P. Automatic hole-filling of triangular meshes using local radial basis function. In: Proceedings of international symposium on 3d data processing, visualization, and transmission; 2006. p. 727–34.

[51] Ju T. Robust repair of polygonal models. ACM Trans Graph 2004;23(3):888–95.

[52] Centin M, Signoroni A. Rameshcleaner: conservative fixing of triangular meshes. In: Proceedings of eurographics Italian chapter conference; 2015. p. 129–38.